Investigation of intrinsic optical damage in potassium bromide at 532 nm

X. A. Shen, Peter Braunlich, and Scott C. Jones
Department of Physics, Washington State University, Pullman, Washington 99164-2814

Paul Kelly
National Research Council, Ottawa, Canada K1A 0R6
(Received 25 January 1988)

We report here the details of an investigation of intrinsic single-pulse optical damage in KBr at 532 nm [Phys. Rev. Lett. **59**, 1605 (1987)]. The technique employed is based on the self-trapped-exciton recombination luminescence, and the temperature dependence of the luminous efficiency is utilized to measure the lattice-temperature rise resulting from the interaction of KBr with intense laser pulses at 532 nm. The mechanism of the laser-solid interaction is shown to be four-photon free-carrier generation and subsequent free-carrier heating with small contributions from laser-generated defect formation, absorption, and relaxation as well as direct recombination of the charge carriers. Single-pulse damage occurs at a temperature very close to the melting point of the material with no indication of electron-avalanche impact ionization.

I. INTRODUCTION

Laser-induced bulk damage of optical materials has been a subject of extensive investigation since the late 1960s. Two mechanisms have been proposed in this subfield of nonlinear optics to describe the interaction of wide-gap solids with intense laser pulses at visible wavelengths: the electron-avalanche theory[1-6] and the alternative multiphoton-polaron theory.[7-9] However, little trustworthy experimental evidence of intrinsic damage exists in support of either mechanism. Earlier work on this subject concentrated on measuring damage thresholds (radiation field strength or laser flux at which damage occurs) as a function of various laser and material parameters, such as initial temperature, incident photon energy, pulse length, interaction volume, etc. Owing to the difficulties in obtaining optical materials of sufficient purity to exhibit intrinsic damage behavior, most of the experiments are at best inconclusive. As was later pointed out by several authors,[10] this method of studying laser-induced damage is neither sensitive nor reliable because it does not provide information about the microscopic processes that contribute to optical damage. Any imperfection of the material, such as inclusions, lattice defects, impurities, etc., can alter the nature of the processes, and hence the damage threshold. In fact, most published damage results reflect only extrinsic damage due to imperfections in the materials.[11,12]

One exception is the recent work by Jones *et al.*,[10] who showed, using a photoacoustic technique, that considerable energy can be deposited into NaCl crystals from intense photon fields at 532 nm, and the lattice-temperature rise resulting from the interaction can be as high as several hundred degrees kelvin without damage. Further, no indication of avalanche formation—hitherto widely believed[1-6] to govern the interaction of wide-gap ionic solids with an intense photon field in the visible wavelength region—was detected. Instead, four-photon free-carrier formation was found to be the primary process of energy deposition from the photon field into the crystal. This work demonstrated for the first time that a prebreakdown study of the laser-solid interaction is a promising approach to the investigation of laser-induced damage of optical materials.

The purpose of this paper is to report prebreakdown temperature measurements in KBr exposed to 532-nm laser pulses. Our results confirm that the primary charge-carrier generation process in this case is also high-order multiphoton absorption with no evidence of electron-avalanche ionization. In addition, we show that the temperature rise resulting from the interaction with the laser pulses is primarily governed by the free-carrier heating mechanism proposed by Epifanov[13] and intrinsic single-pulse damage occurs at a temperature very close to the melting point of the material.

This work is an extension of the earlier investigation by Shen *et al.*[14] of the four-photon absorption cross section in KBr at 532 nm. Self-trapped-exciton recombination luminescence (STERL) is employed in the investigation, and its temperature-dependent efficiency is utilized to monitor the lattice-temperature rise during the interaction with 532-nm laser pulses. This method is new, and data interpretation requires knowledge of the mechanism of charge-carrier generation.

II. THE STERL METHOD

Self-trapped-exciton recombination luminescence is intrinsic to alkali halides.[15] It results from electron-hole (e-h) pair generation (via various excitation processes) and their subsequent radiative recombination. The luminescence yield of self-trapped excitons (STE's) is determined by the formation efficiency of STE's, i.e., the

probability to form a STE per *e-h* pair, and the probability for their radiative decay. The latter depends strongly on lattice temperature.

In most alkali halides, the radiative-decay probability of STE's, or the STE luminescence efficiency, obeys the relation[16]

$$\eta=\frac{1}{1+A\exp(-E/kT)}\ , \tag{1}$$

where E is the activation energy and T the lattice temperature. At low temperatures (below a critical temperature determined by the activation energy E), this efficiency is nearly unity, and it decreases rapidly with increasing T. The STERL method described below utilizes this property of STE's to measure the lattice-temperature rise in KBr resulting from its exposure to intense laser pulses.

The technique requires that the initial temperature of a KBr crystal be below the onset of thermal quenching of STE luminescence. When the crystal is exposed to intense 532-nm laser pulses, *e-h* pairs are created. Since the band gap of KBr is approximately 7.3 eV, larger than the total energy of three photons at 532 nm but less than that of four photons, a valence electron must simultaneously absorb at least four photons to reach the conduction band. Thus, it is a four-photon absorption process. The number of *e-h* pairs generated during the process should be proportional to the fourth power of the incident laser flux, and so should the STE luminescence yield, provided that the lattice temperature stays below the onset of thermal quenching of the luminescence. This has been demonstrated by Shen *et al.*[14] in their measurement of the four-photon absorption cross section in the same material.

However, when the resulting temperature exceeds the onset of thermal quenching, the dependence of the STE luminescence on laser flux will decrease according to $\eta(T)$. In principle, one can obtain directly the temperature rise from the luminescence–versus–photon-flux measurement if one knows $\eta(T)$. However, due to the fact that the incident flux has Gaussian spatial and temporal distributions and thermal quenching does not occur uniformly in the crystal, the procedure of extracting the temperature in the interaction volume becomes much more complicated.

In the absence of thermal quenching, the spatial distribution of laser-induced STE luminescence is proportional to the fourth power of the flux distribution, $F^4(\mathbf{r})$, because the primary excitation process here is four-photon absorption. Any rise in temperature is due to the interaction of laser-generated charge carriers with the photon field;[8,13] its spatial distribution is proportional to $F^4(\mathbf{r})$ as well. When thermal quenching takes place, it first occurs at the center of the interaction volume because there the temperature is highest. Increasing the laser flux enlarges the volume that undergoes thermal quenching as well as the peripheral area that emits luminescence photons. As a result, the detected spatially and temporally integrated luminescence still increases as the photon flux increases even though the emission from the central region is quenched. However, its dependence on photon flux will be less than fourth order.

Knowing how the luminescence distribution changes with photon flux, one can determine the temperature rise from a log-log plot of luminescence yield versus photon flux. The point on the curve at which the slope deviates from 4 indicates that the peak temperature in the interaction volume reaches the onset of thermal quenching. Thus, temperature calibration can be achieved (because its dependence on photon flux remains unchanged). The analysis here provides a direct temperature reading at each flux. However, it can not determine what heating mechanism is responsible for the temperature rise.

Several heating mechanisms have been proposed in the literature (see below) to describe the temperature rise that leads to optical damage; but, prior to the results reported here, there was no direct experimental evidence as to which mechanism is actually operative in any wide-gap materials exposed to intense laser pulses in the visible. Therefore, it will be extremely valuable if one can identify the appropriate heating mechanism for KBr at 532 nm.

Computer simulation allows us to do so. This is possible because, in this case, the four-photon absorption cross section is known.[14] Thus, we can simulate the detected luminescence yield at different laser fluxes for a given heating mechanism and compare it with experiment. By repeating this with different heating mechanisms, we can determine which theory is capable of describing the experimental results. Once this is achieved, the temperature in the interaction volume for any photon flux can be calculated. The details of the analysis are described in Sec. V.

III. EXPERIMENTAL DETAILS

A. Experimental arrangement

The laser system used in our measurements is a Quantronix model 116 Q-switched and mode-locked Nd:YAG laser (here YAG stands for yttrium aluminum garnet) with a double-pass amplifier. A single mode-locked pulse is selected by a pulse selector and converted to 532 nm by a second-harmonic generator. The 532-nm laser pulse is focused into a KBr crystal mounted on a cold finger in a closed-cycle refrigerated optical cryostat operated at 50 K (Fig. 1). A uv-grade optical fiber of 1 mm diameter is used to collect the STE luminescence induced in the interaction volume and guides it to an optical multichannel analyzer for detection. In the experiments, we monitor only the σ component of the STE luminescence for the same reason discussed in Ref. 14.

The samples are reactive-atmosphere-processed [to reduce hydroxyl-ion (OH^-) contamination[17]] ultrapure KBr single crystals obtained from the University of Utah. The size is approximately $4\times4\times25$ mm^3. The front and the back surfaces of the samples are cleaved, and the reflection loss per surface is measured to be approximately 5% at 532 nm. The cold finger, together with the sample, can be moved in the direction perpendicular to the beam axis and that of the fiber so that different interaction sites can be chosen without affecting the collection

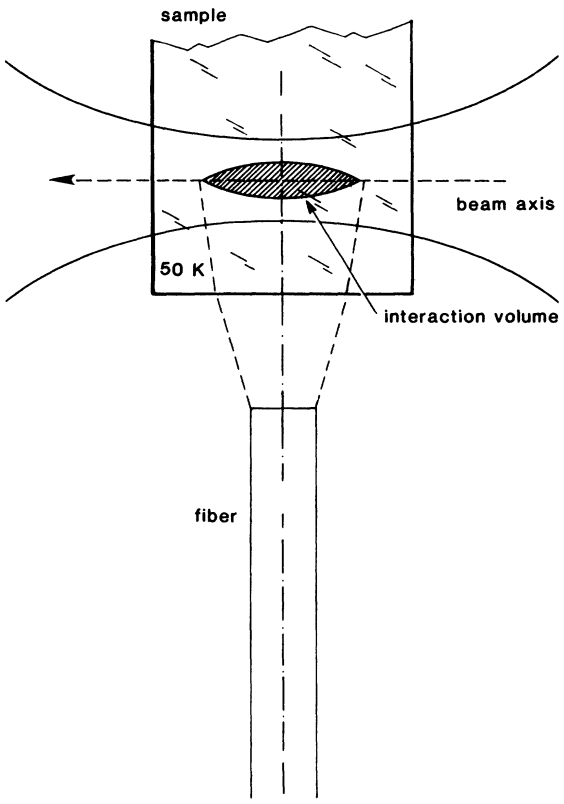

FIG. 1. Experimental arrangement of the luminescence pick-up fiber with respect to the sample and the laser-beam axis. The focal point of the incident laser pulses is located on the axis of the fiber. The sample can be moved in the direction perpendicular to the figure.

efficiency of the fiber. Data are taken by exposing a virgin site to a single laser pulse. This is achieved by moving the sample between pulses.

The details of the experimental arrangement and sample preparation have been described elsewhere.[14]

B. Experimental procedures

Experiments are carried out by carefully monitoring the σ luminescence emitted from the interaction volume as a function of the incident photon flux. Measurements start from relatively low fluxes, where temperature increase is negligible, to the highest flux just prior to any indication of catastrophic damage.

In order to obtain the temperature in the interaction volume from the σ-luminescence-yield–versus–photon-flux relation, careful measurement of the luminous efficiency as a function of lattice temperature is required. This is performed as follows.

We use 266-nm (the fourth harmonic of the Nd:YAG wavelength) laser pulses to produce the σ luminescence in KBr at different sample temperatures and measure its yields for a fixed photon flux. The measurement begins at 50 K, and the higher temperatures are obtained by switching off the refrigerator and letting the sample slowly warm up. Using 266-nm laser pulses precludes any

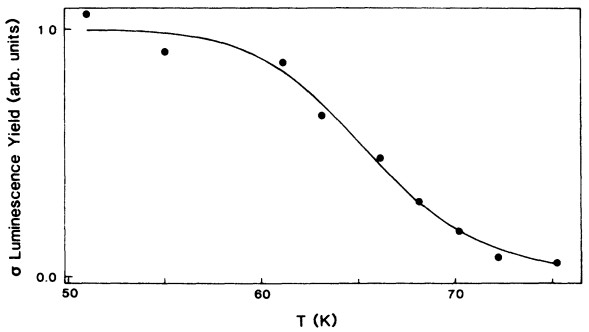

FIG. 2. The σ-luminescence efficiency vs temperature in KBr obtained with single 266-nm laser-pulse excitation. The solid line is the fit to Eq. (1).

temperature rise through the laser-matter interaction, because this process is very efficient for production of STE's (by two-photon absorption[14,18]), but less efficient for energy deposition. Therefore, the measurement reflects more closely the intrinsic efficiency of the σ luminescence.

The measured σ-luminescence efficiency as a function of lattice temperature is given in Fig. 2. Here the dots are the experimental data obtained with single-pulse excitation and the solid line is the fit to Eq. (1) with $A=3.8\times10^{9}$ and $E=0.124$ eV. The results show that thermal quenching occurs above 60 K.

Damage is determined on the basis of two criteria: (a) onset of a broadband emission in addition to the σ luminescence, and (b) the first detectable spatial distortion of the transmitted laser beam. The latter is monitored by looking at the far-field pattern of the laser beam emerging from the sample. Any data obtained with either effect present are considered to represent damage.

The second criterion also provides information about imperfections of the sample surfaces. Since our measurements are carried out at different sample sites, variations of surface quality would introduce, e.g., via beam scattering on nonsmooth surface areas, a large variation in the experimental results because of the highly nonlinear processes. Thus, any exposure to a laser pulse yielding a detectable beam distortion is considered to be due to roughness of either the front or back surface of the sample, or bulk damage. We judge whether damage is intrinsic or extrinsic based on the photon flux at which it occurs.

The onset of broadband emission is chosen as the damage criterion because it is associated with some form of irreversible modification of the material. Experimental evidence is presented in Fig. 3. The upper plot is the σ-luminescence spectrum obtained at a photon flux just above the damage threshold. It shows a slight buildup of broad background emission on the long-wavelength side of the σ peak. The intensity of this emission increases as damage to the material increases; at the same time, the σ-luminescence yield decreases. A typical example of this case is given in Fig. 3(b), which is obtained by reexposing the previously damaged site that yielded Fig. 3(a) to another laser pulse of approximately the same intensity. It shows a clear decrease of the σ-luminescence yield

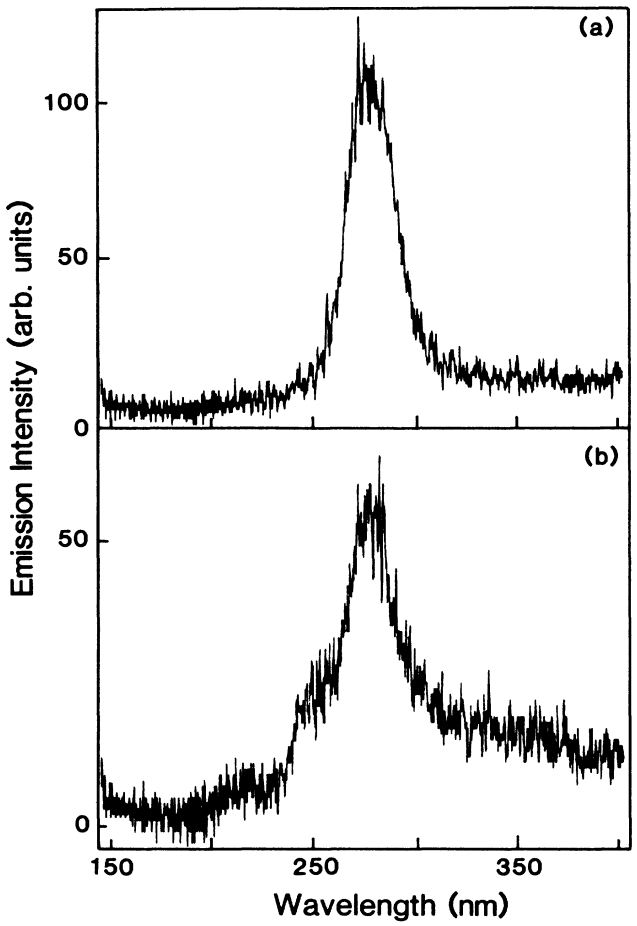

FIG. 3. Broadband emission spectra associated with damage of KBr crystals. The spectrum in (a) was obtained at a flux slightly above the damage threshold. In addition to the σ-luminescence peak, the onset of a clear buildup of background emission at longer wavelengths is detected. The spectrum in (b) was obtained by reexposing the same interaction site to another laser pulse of approximately the same intensity, indicating enhanced background emission.

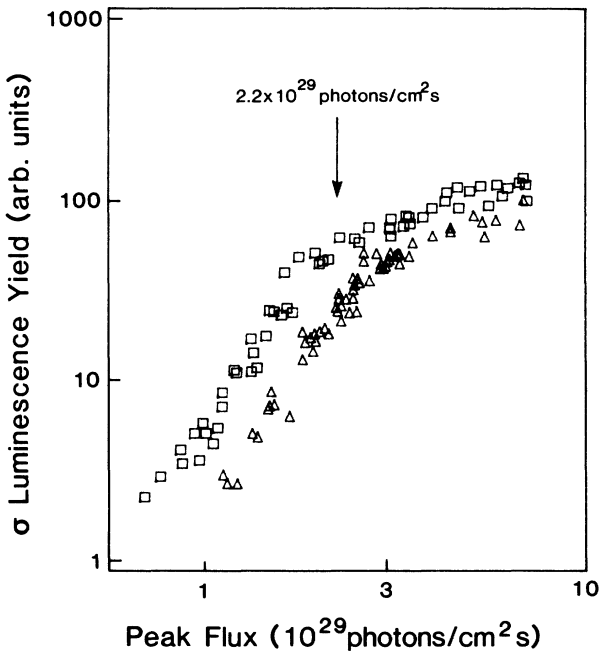

FIG. 4. Total σ-luminescence yield as a function of incident photon flux. The two sets of data (squares and triangles) were obtained from two separate measurements. Both exhibit a sudden decrease of slope at a flux of approximately 2.2×10^{29} photons/cm^2 s. Analysis shows that this is attributed to local temperature rise which results in thermal quenching of the σ luminescence.

along with a substantial increase of the background emission.

The origin of this extraneous emission is unknown. However, it is clearly related to an irreversible modification of the material. We will demonstrate below that the experimental data obtained, using this criterion, along with that of beam deformation, show that single-pulse damage occurs at a temperature very close to the melting point.

We also inspected the samples under a microscope after the measurements using crossed polarizers and did not observe any visual damage, such as crack and bubble formation. Therefore, all the results presented here are considered to be prebreakdown data.

The pulse spatial profile in the sample is obtained by measuring the beam cross section at the focusing-lens position with the slit-scanning technique[14,19] and applying diffraction-limited optics. A typical spot radius (at $1/e$ intensity) at the focal plane is around 5×10^{-4} cm. The pulse length is 100 ps half-width at $1/e$ intensity, measured with the zero-background second-harmonic-generation autocorrelation method.[19] In order to simulate the experimental results for data analysis, we also have to know the collection efficiency of the fiber. This has been described in Ref. 14.

C. Experimental results

The measured σ-luminescence yield versus peak photon flux is plotted on a log-log scale in Fig. 4. At peak fluxes below 2.2×10^{29} photons/cm^2 s, the slope of the curves is approximately 4, as was demonstrated in Ref. 14. Thus, it confirms that the primary electron-hole pair generation process here is indeed four-photon absorption by valence electrons. Furthermore, it indicates that the temperature rise during the interaction is not sufficient to affect the luminous efficiency because; otherwise, the slope would be less than 4. In this flux region, the four-photon absorption cross section is measured to be 2×10^{-112} cm^8 s^3 (Ref. 14).

When the peak flux is above 2.2×10^{29} photons/cm^2 s, strong interaction with the photon field causes the lattice temperature to be higher than the onset of thermal quenching. As a result, the dependence of the σ-luminescence yield on photon flux decreases; it becomes weaker as the flux becomes higher (see Fig. 4). The last

data point in Fig. 4 corresponds to the highest nondamaging flux obtained in the experiments. As will be shown below, the peak temperature at this flux turns out to be very close to the melting point of KBr, 1007 K.

IV. LATTICE HEATING THEORIES

The data presented in the preceding section show a clear temperature rise resulting from the exposure of KBr to the 532-nm laser pulses. The question of what heating mechanism is responsible for it needs to be answered. As we stated earlier, comparison with the available heating theories is our approach to the problem.

Two major heating mechanisms were proposed in the literature to describe the interaction of conduction electrons in wide-gap optical materials with visible laser pulses: the polaron[8] and the free-carrier heating mechanisms.[13] The former assumes that the multiphoton-generated conduction electrons couple strongly to the lattice and any energy gained by the electrons is instantly transferred to the lattice in the form of heat. Those strongly coupled electrons are known as polarons. Thus, according to this theory, the rate of change of lattice energy per unit volume under four-photon excitation is equal to the polaron contribution (via intraband single-photon absorption), $\hbar\omega n_c \sigma_p F$, plus the term $(4\hbar\omega - E_g) N \sigma^{(4)} F^4$. The latter results from the relaxation of the four-photon-generated free electrons to the bottom of the conduction band. These two terms constitute the so-called polaron heating theory. Here ω is the laser frequency, n_c the conduction-electron density, σ_p the polaron absorption cross section, F the photon flux, E_g the band gap, N the density of active atoms (i.e., Br^- ions in our case), and $\sigma^{(4)}$ the four-photon absorption cross section.

According to the free-carrier theory, the main contribution to lattice heating is given by

$$c\rho \frac{dT}{dt} = \frac{\partial}{\partial t}\left[\int_0^{+\infty} \varepsilon n(\varepsilon,t)\, d\varepsilon\right]_+ = 1.09 \left[\frac{m^* kT}{2\pi}\right]^{1/2} \frac{n_c}{l_{ac} v_s} \left[\frac{eE}{m^* \omega}\right]^3 . \quad (2)$$

Here the symbols are c the specific heat, ρ the mass density, ε the kinetic energy of electrons in the conduction band, $n(\varepsilon,t)$ the number of electrons with energy between ε and $\varepsilon + d\varepsilon$ (the solution of the Fokker-Planck diffusion equation used in the free-electron heating theory[13]), l_{ac} the mean free path of conduction electrons with regard to electron-phonon collisions, v_s the longitudinal sound velocity, m^* the band mass of electrons, ω the laser frequency, T the lattice temperature, E the instantaneous amplitude of the electric field, e the electron charge, and k the Boltzmann constant. The $+$ sign denotes that the fraction of the energy responsible for generating additional electrons via avalanche ionization has to be removed from the total energy.

The polaron and the free-carrier heating mechanisms were proposed in the 1970s. However, as we stated earlier, it had not been proven which of them is appropriate to describe the interaction of any optical material with visible laser pulses. Jones *et al.*[17] have shown that both theories could account for their prebreakdown results in NaCl at 532 nm when the four-photon absorption cross section is not precisely known. One of the important results of the present work is that it allowed us to discriminate between them. We will discuss it in the following section.

However, the photon-polaron or photon–free-carrier interaction are not the only mechanisms for energy deposition in nominally transparent ionic solids from intense laser pulses; additional photon absorption by laser-generated primary defects also occurs, and direct nonradiative charge-carrier recombination contributes to heat as well. To discuss these contributions, let us first examine some important processes that are involved in the interaction of KBr with 532-nm laser pulses.

A schematic representation of the relevant electronic transitions in KBr is provided in Fig. 5. Upon four-photon absorption by valence electrons, *e-h* pairs are generated. The hole is simply a neutral Br atom which is effectively positive with respect to the lattice; it tends to interact with a nearest-neighbor Br^- ion to form a Br_2^- molecular ion known as a V_k center. The V_k center is located at the center of two adjacent halogen ion sites with its molecular axis along the $\langle 110 \rangle$ direction. The formation of V_k centers occurs very rapidly (within 10^{-13} s after hole generation[20]), and the process is exothermic. The V_k center may absorb a photon; as a result, it disso-

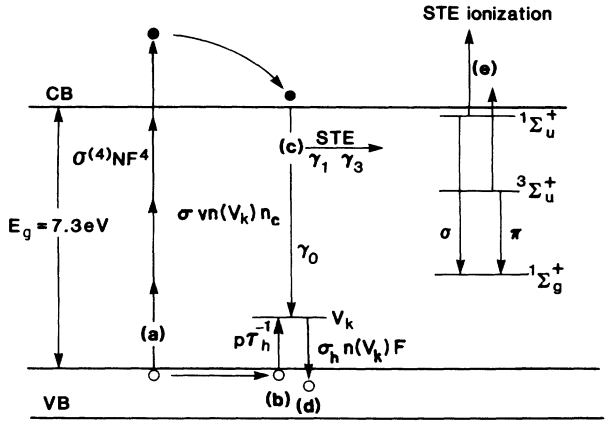

FIG. 5. Energy-level diagram for relevant intrinsic electronic transitions in KBr. The processes can be divided into the following steps. In step (a) four-photon absorption by valence electrons creates electron-hole pairs (dots and circles). The holes bond rapidly to a nearest-neighbor Br^- to form V_k centers as shown by step (b). Trapping of free electrons by V_k centers [step (c)] results in the formation of self-trapped excitons in either the triplet ($^3\Sigma_u^+$) or the singlet ($^1\Sigma_u^+$) state with branching fractions of γ_3 and γ_1, respectively. The remaining portion of the V_k centers and electrons undergo nonradiative recombination, which is indicated by γ_0. In steps (d) and (e), the V_k center and STE's absorb photons; as a result the V_k center dissociates, leaving a free hole in the valence band, while STE's are ionized as shown by the upward arrows.

ciates and returns back to the normal lattice configuration with a free hole in the valence band. The V_k center has a large cross section for electron capture. Electron trapping by V_k centers results in the formation of STE's in either the triplet ($^3\Sigma_u^+$) or the singlet ($^1\Sigma_u^+$) state with formation efficiencies γ_3 and γ_1, respectively. Radiative transition of an electron from $^3\Sigma_u^+$ to the ground state ($^1\Sigma_g^+$) of STE's gives rise to the π luminescence, while the σ luminescence stems from the transition $^1\Sigma_u^+ \rightarrow {}^1\Sigma_g^+$. Electrons and V_k centers may recombine nonradiatively by phonon emission or production of primary defects, such as F and H centers (an F center is an electron bound to a negative-ion vacancy, while an H center is a singly ionized halogen molecule occupying a negative-ion site). The probability γ_0 for this process to occur is equal to $1-\gamma_1-\gamma_3$. With the above-mentioned photochemical processes in mind, we can now proceed to discuss their contribution to the lattice heating.

The lattice can gain energy through formation of V_k centers; its rate per unit volume can be written as $\varepsilon_h p \tau_h^{-1}$, where ε_h is the binding energy of a V_k center, p the free-hole density, and $\tau_h = 10^{-13}$ s, the time for a hole to be trapped in a V_k-center configuration. However, ε_h for KBr is not known. Gilbert[21] estimated the binding energy of Cl_2^- in KCl to be approximately 1.5 eV. We choose this value for ε_h in our calculation to compute the energy deposition into the lattice via V_k-center formation. The error introduced with this approximation is estimated to be very small, the reason for which will become clear as our discussion proceeds.

Dissociation of a V_k center via photon absorption also releases energy. The resulting free hole is, of course, retrapped again within 10^{-13} s. The total energy released during the process (dissociation and subsequent reformation of the V_k center) is equal to the photon energy $\hbar\omega$ absorbed by the V_k center. Since the formation energy is ε_h, the energy gained by the lattice due to dissociation of a V_k center is $\hbar\omega - \varepsilon_h$, contributing the term $(\hbar\omega - \varepsilon_h)\sum_{i=1}^{3}\sigma_{hi} n(V_{ki})F$, to the total heating rate. Here σ_{hi} and $n(V_{ki})$ are the absorption cross section and density of V_k centers of different orientations.[14] Since V_k-center dissociation via photon absorption is always associated with its immediate reformation, and the energy gained in this process is equal to the absorbed photon energy, it is clear now why the absolute value of ε_h is not critical. We will further show below that the contribution to lattice heating from V_k centers is much smaller compared to that from free-carrier heating. Therefore, a slight uncertainty in ε_h will not affect our calculation.

According to Fig. 5, the heating due to direct nonradiative recombination of V_k centers and electrons is equal to $(E_g - \varepsilon_h)\gamma_0 \sigma v n(V_k) n_c$, where σ is the cross section for electron capture by V_k centers and v the average thermal velocity of conduction electrons.

Formation of a triplet STE also gives off heat. Williams *et al.*[22] have estimated that the depth of the triplet state of STE's below the conduction band is approximately 2.3 eV for KBr. Thus, the energy released upon its formation is $\varepsilon_3 \approx 2.3$ eV. Similarly, the energy gained by the lattice from formation of a singlet STE is $\varepsilon_1 = \varepsilon_3 - (\hbar\omega_\sigma - \hbar\omega_\pi)$. Here the term in parentheses is the energy difference between the σ- and π-luminescence photons.

The ground state of STE's is that of antibonding molecular ions,[23] and is unstable. The dissociation of STE's in this state (upon radiative decay from the triplet or singlet state) will also release energy, and it is estimated, from conservation of total energy, to be $\varepsilon_d \approx E_g - \varepsilon_3 - \hbar\omega_\pi - \varepsilon_h$. Thus, the rates of energy gained by the lattice per unit volume resulting from radiative and nonradiative decay of the triplet and singlet STE's are

$$[\varepsilon_d \eta_3 + (\hbar\omega_\pi + \varepsilon_d)(1-\eta_3)] S_3 \tau_3^{-1}$$

and

$$[\varepsilon_d \eta_1 + (\hbar\omega_\sigma + \varepsilon_d)(1-\eta_1)] S_1 \tau_1^{-1} .$$

Here η is the efficiency of the STE luminescence, and S and τ are the density and lifetime of the STE's. The subscripts 3 and 1 denote those parameters for the triplet and singlet STE's, respectively. The second term in both expressions is the contribution from their nonradiative decay.

One more channel for lattice heating is the ionization of a STE in the triplet or singlet state by absorption of a laser photon and subsequent relaxation to the bottom of the conduction band. The energy transferred to the lattice through this channel is $\hbar\omega - \varepsilon_3$ for the ionization of a triplet STE and $\hbar\omega - \varepsilon_1$ for that of a singlet STE. Therefore, the total contribution to lattice heating (rate of change of lattice energy per unit volume) from direct charge-carrier recombination as well as defect formation, ionization, and relaxation can be summarized as

$$\begin{aligned} W = {} & \varepsilon_h p \tau_h^{-1} + (\hbar\omega - \varepsilon_h)\sum_{i=1}^{3}\sigma_{hi} n(V_{ki}) F + (E_g - \varepsilon_h)\gamma_0 \sigma v n(V_k) n_c + \varepsilon_3 \gamma_3 \sigma v n(V_k) n_c + \varepsilon_1 \gamma_1 \sigma v n(V_k) n_c \\ & + [\varepsilon_d \eta_3 + (\hbar\omega_\pi + \varepsilon_d)(1-\eta_3)] S_3 \tau_3^{-1} + [\varepsilon_d \eta_1 + (\hbar\omega_\sigma + \varepsilon_d)(1-\eta_1)] S_1 \tau_1^{-1} \\ & + (\hbar\omega - \varepsilon_3)\sum_{i=1}^{3}\sigma_{3i} S_{3i} F + (\hbar\omega - \varepsilon_1)\sum_{i=1}^{3}\sigma_{1i} S_{1i} F . \end{aligned} \tag{3}$$

Thus, the polaron heating theory can be written as

$$c\rho \frac{dT}{dt} = (4\hbar\omega - E_g) N \sigma^{(4)} F^4 + \hbar\omega \sigma_p n_c F + W , \tag{4}$$

and the free-carrier theory as

$$c\rho \frac{dT}{dt} = 1.09 \left[\frac{m^* kT}{2\pi}\right]^{1/2} \frac{n_c}{l_{ac} v_s} \left[\frac{eE}{m^* \omega}\right]^3 + W . \tag{5}$$

Here both theories disregard the energy loss due to formation of stable defects, such as F centers, in alkali halides. Simple calculation shows that it is indeed negligible compared to the total energy gained by the lattice.[19]

V. MODEL CALCULATIONS

A set of rate equations describing the transitions of electrons in KBr under 532-nm laser-pulse excitation at 50 K was provided by Shen *et al.*[14] The calculation performed below is based on those equations with some modifications. First, the temperature dependence of all the parameters has to be considered since the calculation is extended to higher temperature (up to 1007 K). Second, certain processes, such as diffusion of charge carriers and defects, which were not important at low temperature, need to be reexamined.

The calculation relies on the σ-luminescence efficiency. This parameter has been carefully measured at different temperatures and has been shown to obey Eq. (1) (see Sec. III). The efficiency of the π luminescence does not, however, follow Eq. (1) exactly due to its band splitting.[14,19] It exhibits a slight increase prior to its onset of thermal quenching at approximately 50 K, but, aside from this, it behaves very much like the σ-luminescence efficiency. As stated earlier, only the σ luminescence is monitored in the experiments and, consequently, only the σ-luminescence yield needs to be precisely computed. Employing an approximation for the π-luminescence efficiency will not affect the calculation of the σ luminescence because the triplet and the singlet STE's are independent entities. We assume that the π-luminescence efficiency approximately follows Eq. (1) with $A=1.5\times10^{10}$ and $E=0.126$ eV (Ref. 19). The remaining question is whether or not the use of the imprecise π-luminescence efficiency would affect the temperature calculation by underestimating or overestimating the contribution from the triplet STE's to the lattice heating. As will be shown below, even the total contribution from STE's (π plus σ, radiative and nonradiative) is negligible compared to the contribution from free carriers and V_k centers. Thus, the approximation for the π-luminescence efficiency is justified.

In the original polaron heating model proposed by Schmid *et al.*,[8] the photon–conduction-electron interaction is assumed to be dominated by scattering with acoustic phonons. These authors used the expression by Pokatilov and Fomin[24] to estimate polaron absorption cross sections in their calculations of damage thresholds for some alkali halides. Here we choose the Huybrechts-Devreese expression[25] for the polaron absorption cross section:

$$\sigma_p \approx \left[\frac{4\pi e^2}{nc_l m^* \omega_0}\right]\left[\frac{2\alpha}{3}\right]\left[\frac{\omega_0}{\omega}\right]^{5/2} \times\left[1+\frac{2}{\exp(\hbar\omega_0/kT)-1}\right], \tag{6}$$

where ω_0 is the optical phonon frequency, m^* the band mass, α the polaron coupling constant, ω the laser frequency, n the refractive index, c_l the speed of light, and T the lattice temperature. This expression is valid for all temperatures and values of the coupling constant under the condition of $\omega/\omega_0 \gg 1$. The reason for doing so is that both the Huybrechts-Devreese and the Pokatilov-Fomin theories give a very similar value for σ_p in the temperature region of interest, yet the computational effort required in using the latter is significantly greater.

The lifetimes of STE's in both the triplet and the singlet states are chosen to be constant and their values at 50 K are used in the calculation.[26] The error introduced with this approximation is very small because the σ luminescence occurs only in a narrow temperature range from 50 to 60 K, in which the lifetimes do not change significantly.

Epifanov[13] calculated the electron diffusion in NaCl (with optical and thermal properties similar to KBr) exposed to 532-nm laser pulses and found its coefficient to be approximately 30 cm^2/s. We estimated, using this value, the electron diffusion in KBr and found it to be negligible under our experimental conditions (spot radius $w_0 \approx 5\times10^{-4}$ cm, and pulse length $\tau=10^{-10}$ s). Similar conclusions can be derived for the diffusion of V_k centers and STE's using the results reported by Tanimura and Itoh.[27] Thermal diffusion and beam deformation are also neglected in our calculation, the reason for which has been discussed elsewhere.[14,17]

A. Computational method

Due to the complexity of the model equations (Ref. 14), direct integration over measured pulse profiles to obtain spatially and temporally integrated σ-luminescence yield as a function of peak photon flux is not economical. It would require this complicated computation to be repeated for each data point. To simplify the calculation, let us first examine the laser pulses used in the experiments as well as the model equations in the calculation. The laser-pulse profile is Gaussian in both time and space; mathematically, it can be written as

$$\begin{aligned} F(\mathbf{r},t) &= F(\mathbf{r})\exp\left[-\frac{t^2}{\tau^2}\right] \\ &= \frac{F_p}{(1+z^2/z_0^2)}\exp\left[-\frac{r^2}{w_0^2(1+z^2/z_0^2)}\right] \\ &\quad\times\exp\left[-\frac{t^2}{\tau^2}\right], \end{aligned} \tag{7}$$

where $F_p=F(0,0)$, w_0 is the Gaussian beam waist, z_0 the confocal parameter ($z_0=2\pi\omega_0^2 n/\lambda$), $F(\mathbf{r})$ the spatial distribution of the laser flux, and τ the pulse length. The model equations do not contain explicitly spatial variables. Thus, we can divide the calculation into two steps. In step 1 we solve the rate equations with a time-dependent photon flux $F(t)=F_0\exp(-t^2/\tau^2)$, and obtain

TABLE I. Parameter values in the model calculation.

Symbol	Value
ω_0	3.13×10^{13} s^{-1}
m^*	$0.388m_e$
α	3.16
l_{ac}	3.0×10^{-7} cm
v_s	3.15×10^{5} cm/s

the time-integrated σ-luminescence yield as a function of F_0. Then we fit the calculated results to an appropriate function (see below). This function thus provides us with a time-integrated σ-luminescence yield at any arbitrary point in the interaction volume after exposure to an intense 532-nm laser pulse whose peak flux at this point is F_0. Once this function is obtained, we proceed with step 2, in which we replace F_0 by the measured laser spatial profile $F(\mathbf{r})$, and integrate the function over the entire space for different F_p to obtain the spatially and temporally integrated σ-luminescence yield as a function of F_p. The results can now be compared directly to the measurements. With the above approach, the spatial integration does not require solving the model equations for every point in the interaction volume, which considerably simplifies the calculation. It should be pointed out that this approach is not an approximation; it is just a simplified method for computing the total luminescence yield.

For computational convenience, we express the laser pulse as $F(\mathbf{r},t)=F(\mathbf{r})\exp[-(t-\sqrt{5}\tau)^2/\tau^2]$. The calculation starts at $t=0$ and is stopped when the σ-luminescence emission and temperature rise are completed. Some parameter values used in our calculations are listed in Table I, and the rest are the same as those given in Ref. 14. The temperature-dependent specific heat is taken from the Debye theory with Debye temperature of 173 K.[28]

B. Computational results

In Fig. 6, the results for the temporally integrated σ-luminescence yield, calculated in step 1, are plotted as a function of photon flux for both the polaron and free-carrier heating theories. At low flux the σ-luminescence yield $L^{(1)}$ increases as the flux increases and follows the expected fourth-order dependence. In the model based on the polaron theory (dots in Fig. 6), the onset of thermal quenching occurs at $F_0=3.7\times10^{29}$ photons/cm^2 s at which the peak of $L^{(1)}$ is reached. The luminescence yield decays rapidly at higher fluxes. In the free-carrier heating model (triangles in Fig. 6), however, the onset of thermal quenching occurs at 2.2×10^{29} photons/cm^2 s, much earlier than that in the polaron case. The calculated data points for both models are fitted to the function

$$L^{(1)}=\left[\frac{1-\exp(-AF_0^4)}{1+B\exp(-C/F_0^4)}\right], \tag{8}$$

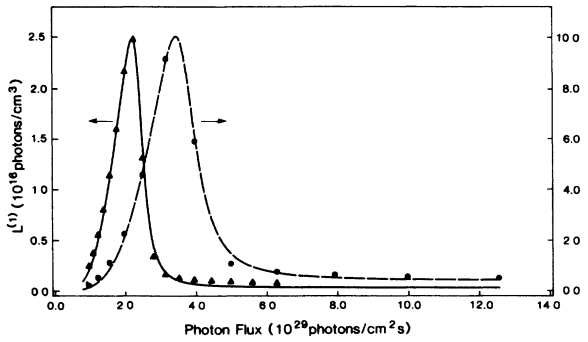

FIG. 6. Time-integrated σ-luminescence yield, calculated using the polaron (dots) and free-carrier (triangles) heating theories, as a function of photon flux. The solid and dashed lines are the best fits obtained using Eq. (8). At relatively low fluxes the integrated luminescence yield is proportional to the fourth power of the flux. Thermal quenching sets in at the peaks of the curves.

which is the time-integrated σ-luminescence yield per unit volume. This function has the expected properties, namely it is proportional to F_0^4 at fluxes for which thermal quenching is negligible and levels off to a very small value at very high fluxes. The fact that it does not reach zero is due to the emission at the beginning of each pulse before the temperature exceeds about 60 K. The fitted results are given by the solid and dashed lines in Fig. 6. The total (spatially and temporally integrated) luminescence yield collected by the optical fiber as a function of F_p, the peak flux of the laser pulse, is given by (step 2)

$$L^{(1)}_{\text{total}}(F_p)=\int_V P(z)\left[\frac{1-\exp(-AF^4)}{1+B\exp(-C/F^4)}\right]dV\ , \tag{9}$$

where F is $F(\mathbf{r})$ in Eq. (7) and $P(z)$ is the probability for the fiber to collect a photon emitted from a source at z along the beam axis (see Fig. 1 and Ref. 14).

The calculated results of $L^{(1)}_{\text{total}}$ versus F_p are compared with experimental data in Fig. 7. Here the dashed line is obtained with the polaron heating theory, while the solid line is calculated with the free-carrier theory. The vertical axis is the total number of photons collected by the optical fiber. The experimental results are normalized by fitting those below $F_p=2.2\times10^{29}$ photons/cm^2 s to the calculated curves, because in this region the temperature effect does not influence the dependence on photon flux in either theory, and the experimental results should follow the predictions of both theories.

The comparison in Fig. 7 clearly shows that the free-carrier heating theory readily accounts for the experimental results, while the polaron theory does not. To ensure that the polaron heating theory indeed fails to explain the temperature rise observed here, we repeated the computation with σ_p values up to 2 orders of magnitude larger. Polaron heating is still too inefficient to account for the thermal quenching occurring at 2.2×10^{29} photons/cm^2 s. The calculation of the σ-luminescence

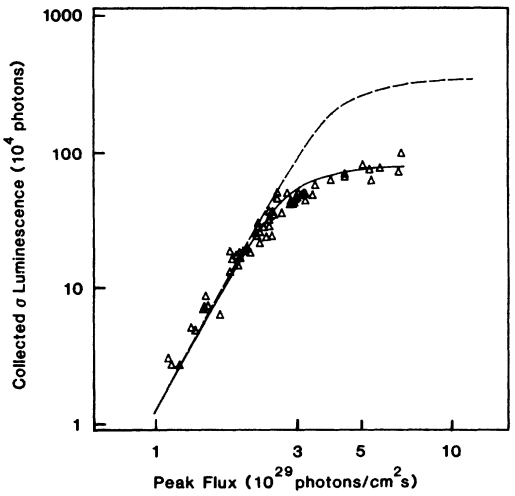

FIG. 7. Calculated (solid and dashed lines) and measured (triangles) spatially and temporally integrated σ-luminescence emission from KBr as a function of the peak photon flux in 532-nm laser pulses of 100-ps duration ($1/e$ intensity half-width). The solid line is obtained using the free-carrier heating model, while the dashed line is based on the polaron heating model.

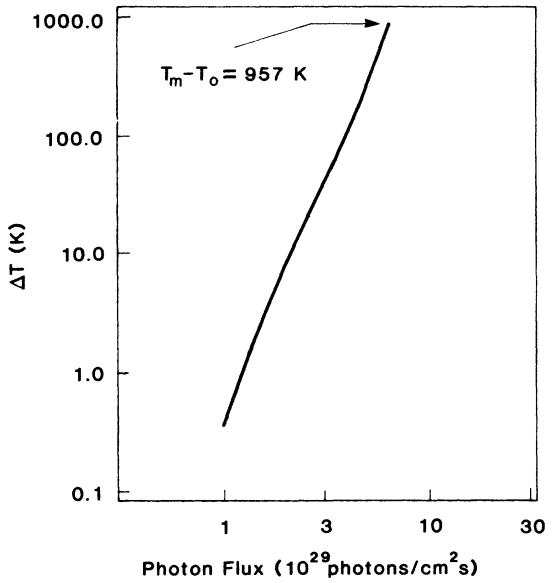

FIG. 8. Calculated peak temperature rise as a function of photon flux in the interaction volume of KBr exposed to single 532-nm pulses of 100-ps $1/e$ half-width. Here T_m and T_0 are the melting and initial temperatures, respectively. The slope of the curve is approximately 4, whereby slight deviations are mainly due to the temperature dependence of the specific heat.

yield versus photon flux is stopped when the peak temperature reaches the melting point. In the entire flux region, the agreement between the experimental results and the free-carrier heating theory is very satisfactory.

The above calculations are based on the assumption that the primary charge-carrier generation process up to damage is four-photon absorption. This is clear at lower photon fluxes (below 2.2×10^{29} photons/cm^{2}s), but whether it is still so at higher fluxes requires some analysis.

According to the calculation, the last data point in Fig. 7 corresponds to a peak temperature of 918 K, which provides a lower limit because any other conceivable process, e.g., avalanche ionization, would result in a higher temperature. On the other hand, we did not observe any catastrophic damage of the material up to this flux, which ensures that the temperature in the interaction volume has to be below the melting point. Thus, if any other contribution to the lattice heating, such as avalanche formation, were present, it would have to be less than 89 K. We can conclude, therefore, that the energy-deposition process in the case of KBr exposed to 532-nm laser pulses up to melting is dominated by four-photon-generated free-carrier heating.

The above finding is very important. It is the first experimental evidence that the melting point can indeed be reached via four-photon absorption without electron-avalanche formation. We take this and the fact that the measured prebreakdown phenomena can be explained by the theory described above as direct evidence that the interaction of intense 532-nm laser pulses with KBr is intrinsic in nature and not influenced by crystal imperfections or impurities.

With the experimental evidence that free-carrier heating is the appropriate mechanism for energy deposition in the case of KBr exposed to 532-nm laser pulses, the peak-temperature-rise–versus–laser-flux relation can now be calculated with confidence and is shown in Fig. 8. The dependence of the peak temperature on photon flux is approximately fourth order, as expected.

The uncertainty of the calculated temperature can be estimated from Fig. 7, where the luminescence serves as a thermometer, and the fit to the experimental results is the calibration. The calculation of the temperature is based on this fit. Thus, estimating the uncertainty in temperature reduces to estimating the error in data fitting. The latter can be done by varying the adjustable parameters (e.g., l_{ac}, v_s, or m^*) in Eq. (5) or, equivalently, moving the solid curve in Fig. 7 along the dashed line in either direction, and examining the maximum allowable deviation from the calculation $\Delta(\log_{10}F_p)$, which still provides a reasonable fit. By determining $\Delta(\log_{10}F_p)$, we can calculate the uncertainty in temperature from Fig. 8. Our results show that at the last data point, which corresponds to a temperature of 918 K, the uncertainty is less than 30%.

Our calculation shows that heating of four-photon-generated free carriers [the first term in Eq. (5)] dominates the energy deposition in the case of KBr, contributing 93.3% of the heat to the lattice at $F_p=6.3\times10^{29}$ photons/cm^{2}s. Only 6.7% of the heat stems from direct charge-carrier recombination and laser-generated defect absorption and relaxation, less than one-tenth of which results from relaxation and ionization of STE's. The main contribution of W to lattice heating is due to V_k-center ionization and subsequent reformation.

The time-integrated σ-luminescence and temperature

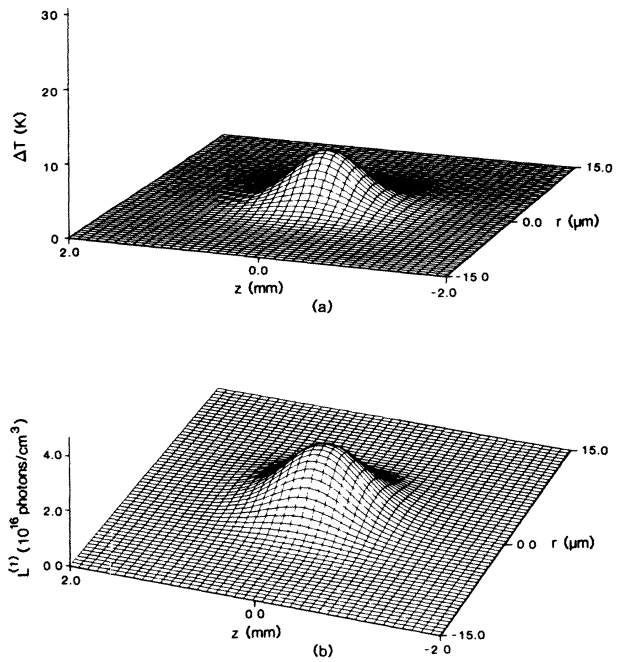

FIG. 9. (a) Temperature and (b) spatially resolved time-integrated σ-luminescence distributions in KBr immediately after exposure to a single 532-nm pulse of peak flux 2.0×10^{29} photons/cm^2 s. The beam axis is the z axis and r is the radius in cylindrical coordinates from the optical axis. The geometrical focal point is $(r,z)=(0,0)$. Note different scales of axes.

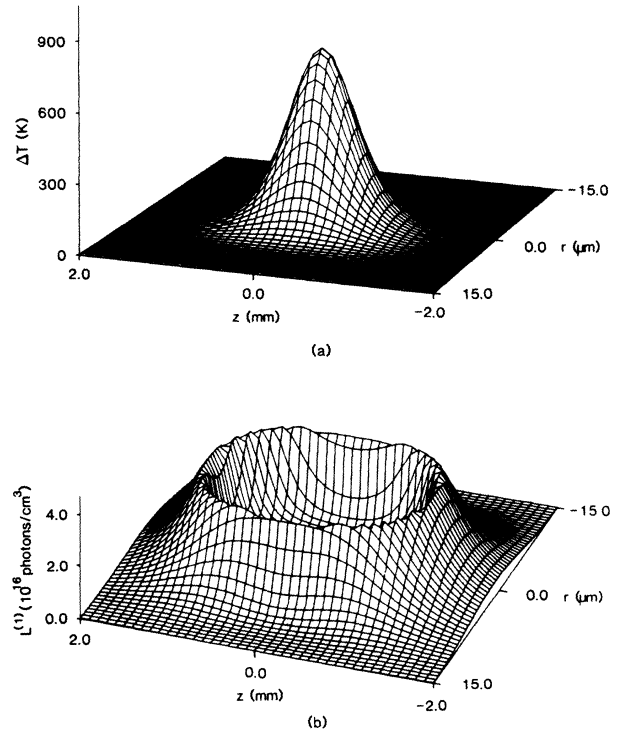

FIG. 10. Same as Fig. 9, but with a peak flux of 6.3×10^{29} photons/cm^2 s, the highest prebreakdown value obtained.

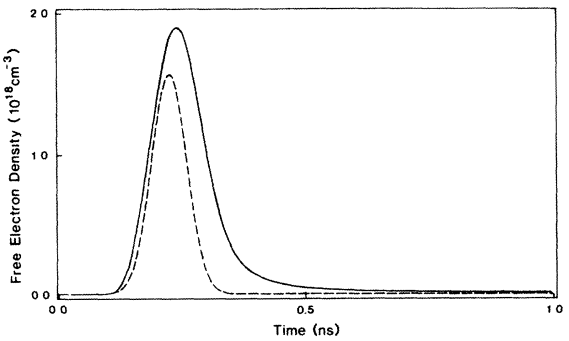

FIG. 11. Time-dependent free-carrier density under excitation of a single 532-nm pulse of peak flux 6.3×10^{29} photons/cm^2 s, which corresponds to a peak temperature rise of 918 K. Here the peak density reached at this flux is 1.9×10^{18} cm^{-3}. The dashed line is the fourth power of peak flux, F_p^4, vs time in arbitrary units.

distributions, immediately after a laser pulse has passed through the interaction volume for a typical spatial pulse profile, are given in Figs. 9 and 10. At a flux below 2.2×10^{29} photons/cm^2 s (Fig. 9), the temperature rise is too small to influence the σ-luminescence efficiency, and the temperature and luminescence distributions have approximately the same shape, namely the fourth power of the laser-flux distribution. When the laser flux exceeds this value, however, the temperature at the center of the interaction volume rises above the onset of thermal quenching (60 K). Thus, in this region the σ-luminescence yield is reduced, resulting in a distribution whose shape differs from that of the temperature distribution. An example is shown in Fig. 10 for a laser peak flux $F_p=6.3\times10^{29}$ photons/cm^2 s. Here the total σ-luminescence yield is determined by the regions of the spatial distribution where the flux level is below 2.2×10^{29} photons/cm^2 s. The regions with higher fluxes undergo thermal quenching, resulting in the distribution shown in Fig. 10(b). The fraction of the volume in which the luminescence is quenched increases as the peak flux of the pulse increases, until the peak temperature reaches the melting point. Then catastrophic damage of the material occurs.

The time evolution of the free-electron density for a pulse of peak flux $F_p=6.3\times10^{29}$ photons/cm^2 s (which corresponds to the peak temperature of 918 K) is calculated, from the free-carrier heating theory, and plotted in Fig. 11. The peak density reached is 1.9×10^{18} electrons/cm^3 which, incidentally, agrees with the damage criterion of 10^{18} electrons/cm^3 used in the earlier theoretical study of optical damage.[1-6]

VI. SUMMARY AND CONCLUSIONS

We have demonstrated, using the STERL method, that the primary interaction process in KBr exposed to intense 532-nm laser pulses is governed by four-photon free-carrier generation and subsequent photon absorption by free carriers with small contributions from laser-

generated primary defect formation, ionization, and recombination as well as direct charge-carrier recombination. The lattice heating process is shown to occur according to the heating mechanism proposed by Epifanov.[13] The highest temperature reached in the interaction volume via four-photon-generated free-carrier absorption just prior to any indication of catastrophic damage is approximately the melting point of the material, which demonstrates that melting is indeed indicated as a failure mode of the optical material.

However, the damage mechanism identified here pertains only to KBr at the particular laser wavelength. It is not a general finding and, therefore, may not be applied to other optical materials; but it is probably safe to extend our conclusion to most alkali halides at the same order of multiphoton process because of the very similar material properties in these solids. However, caution must still be taken in dealing with each individual case.

Predicting damage behavior under different conditions using the identified theory and designing experiments to test its validity must be the subject of further investigations. Recent work by our group indicates good agreement between theory and preliminary experimental results. However, additional work is necessary. This will be presented in a forthcoming publication.

Our experiments show that the STERL method is a promising tool for the investigation of high-order nonlinear interaction processes in alkali halides. It allows one to study both the primary free-carrier generation and the energy-deposition processes in these materials as a consequence of nonlinear interaction with intense photon fields. Therefore, it should be useful in future work on optical damage. However, some peculiarities among the alkali halides, such as the absorption bands of the STE's, may interfere with its application, since it may be possible to bleach the STE luminescence with laser photons. A careful matching of laser wavelength with the particular material of interest is called for.

ACKNOWLEDGMENTS

We would like to thank Mr. R. Thomas Casper for his valuable assistance. This work was supported by the U.S. Air Force Office of Scientific Research under Grant No. AFOSR-87-0081.

[1]W. L. Smith, Opt. Eng. **17**, 489 (1978).
[2]S. Brawer, Phys. Rev. B **20**, 3422 (1979).
[3]M. Sparks, D. L. Mills, R. Warren, Y. Holstein, A. A. Maradudin, L. J. Sham, E. Loh, Jr., and D. F. King, Phys. Rev. B **24**, 3519 (1981).
[4]N. Bloembergen, IEEE J. Quantum Electron. **QE-10**, 375 (1974).
[5]A. S. Epifanov, IEEE J. Quantum Electron. **QE-17**, 2018 (1981).
[6]B. G. Gorshkov, A. S. Epifanov, and A. A. Manenkov, Zh. Eksp. Teor. Fiz. **76**, 617 (1979) [Sov. Phys.—JETP **49**, 309 (1979)].
[7]P. Braunlich, A. Schmid, and P. Kelly, Appl. Phys. Lett. **26**, 150 (1975).
[8]A. Schmid, P. Kelly, and P. Braunlich, Phys. Rev. B **16**, 4569 (1977).
[9]P. Kelly, A. Schmid, and P. Braunlich, Phys. Rev. B **20**, 815 (1979).
[10]Scott C. Jones, X. A. Shen, P. Braunlich, P. Kelly, and A. S. Epifanov, Phys. Rev. B **35**, 894 (1987).
[11]E. W. Van Stryland, M. J. Soileau, A. L. Smirl, and William E. Williams, in *Laser-Induced Damage in Optical Materials*, Natl. Bur. Stand. (U.S) Spec. Publ. No. 620, edited by H. E. Bennett, A. J. Glass, A. H. Guenther, and B. E. Newnam (U.S. GPO, Washington, D.C., 1981), pp. 375–384.
[12]A. A. Manenkov, in *Laser-Induced Damage in Optical Materials*, Natl. Bur. Stand. (U.S) Spec. Publ. No. 509, edited by A. J. Glass and A. H. Guenther (U.S. GPO, Washington, D.C., 1978), pp. 455–464.
[13]A. S. Epifanov, Zh. Eksp. Teor. Fiz. **67**, 1805 (1974) [Sov. Phys.—JETP **40**, 897 (1975)].
[14]X. A. Shen, Scott C. Jones, P. Braunlich, and P. Kelly, Phys. Rev. B **36**, 2831 (1987).
[15]M. N. Kabler, Phys. Rev. **136**, A1296 (1964).
[16]M. Ikezawa and T. Kojima, J. Opt. Soc. Jpn. **27**, 1551 (1969).
[17]Scott C. Jones, A. H. Fischer, Peter Braunlich, and Paul Kelly, Phys. Rev. B **37**, 755 (1988).
[18]P. Liu, W. L. Smith, H. Lotem, J. H. Bechtel, N. Bloembergen, and R. S. Adhav, Phys. Rev. B **17**, 4620 (1978).
[19]X. A. Shen, Ph.D. dissertation, Washington State University, 1987.
[20]R. T. Williams, J. N. Bradford, and W. L. Faust, Phys. Rev. B **18**, 7038 (1978).
[21]W. B. Fowler, in *Physics of Color Centers*, edited by W. B. Fowler (Academic, New York, 1968).
[22]R. T. Williams and M. N. Kabler, Phys. Rev. B **9**, 1897 (1974).
[23]Ch. B. Lushchik, in *Excitons*, edited by E. I. Rashba and M. D. Sturge (North-Holland, New York, 1982).
[24]E. P. Pokatilov and V. M. Fomin, Phys. Status Solidi B **73**, 553 (1976).
[25]W. Huybrechts and J. Devreese, in *Elementary Excitations in Solids, Molecules and Atoms*, edited by J. Devreese, A. B. Kunz, and T. C. Collins (Plenum, New York, 1974), Vol. B.
[26]S. Wakita, Y. Suzuki, H. Ohtani, S. Tagawa, and M. Hirai, J. Phys. Soc. Jpn. **50**, 3378 (1981).
[27]K. Tanimura and N. Itoh, J. Phys. Chem. Solids **42**, 901 (1981).
[28]N. W. Ashcroft and N. D. Mermin, *Solid State Physics* (Saunders College, Philadelphia, 1976).

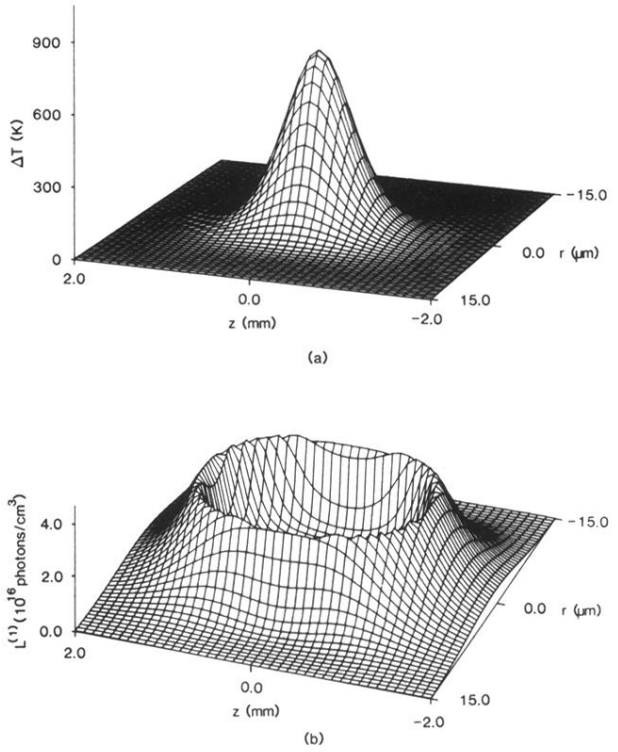

FIG. 10. Same as Fig. 9, but with a peak flux of 6.3×10^{29} photons/cm^2 s, the highest prebreakdown value obtained.